Towards Shape-Adaptive Attachment Design for Wearable Devices Using Granular Jamming

Joseph Brignone, Logan Lancaster, Edoardo Battaglia, *Member, IEEE*, and Haohan Zhang, *Member, IEEE*

***Abstract*—Attaching a wearable device to the user's body for comfort and function while accommodating the differences and changes in body shapes often represents a challenge. In this letter, we propose an approach that addresses this problem through granular jamming, where a granule-filled membrane stiffens by rapidly decreasing the internal air pressure (e.g., vacuum), causing the granule material to be jammed together due to friction. This structure was used to conform to complex shapes of the human body when it is in the soft state while switching to the rigid state for proper robot functions by jamming the granules via vacuum. We performed an experiment to systematically investigate the effect of multiple design parameters on the ability of such jamming-based interfaces to hold against a lateral force. Specifically, we developed a bench prototype where modular granular-jamming structures are attached to objects of different sizes and shapes via a downward suspension force. Our data showed that the use of jamming is necessary to increase the overall structure stability by 1.73 to 2.16 N. Furthermore, using three modules, high suspension force, and a low membrane infill (∼25%) also contribute to high resistance to lateral force. Our results lay a foundation for future implementation of wearable attachments using granular-jamming structures.**

***Index Terms*—Wearable robotics, granular jamming, physical human-robot interaction.**

I. Introduction

WEARABLE devices such as exoskeletons and powered prostheses have been widely used to quantify movements [1], enhance performance, and assist with impaired motor functions [2]. Despite their success, fitting a wearable device on people comfortably while maintaining the device's function and stability remains a great challenge [3]. Currently, one of the most common techniques is to use plastic cuffs that are shaped like the human body contour for interfacing the device and the body. Then, straps are added to fasten the semi-rigid cuff on the body, maintaining device-on-body stability. However, as body shapes are widely different among users, cuffs with generic shapes cannot fully mesh with the body shape of an individual, resulting in high tightening force of the straps to maintain stability [4]. Even with customized padding (e.g., foam), adverse events like device-on-body motion still often occur, which significantly reduces comfort and limits device functions [5].

To improve fitting, personalized cuffs can be designed and then fabricated based on a 3D body scan [6], [7]. Material like thermoplastic can also be used to mold the cuffs into an individual user's body shape [8]. However, time, expertise, additional cost, and special tools may be required to accomplish this, which limits accessibility and usability. These challenges become more profound when repeating these procedures is necessary.

For example, the body shape can evolve over time due to factors like growth (e.g., children), aging, or neurodegenerative diseases (e.g., amyotrophic lateral sclerosis). By contrast, it is also possible to permanently integrate the device with the human body directly through means like surgical modification of the body [9], [10]. However, such an approach comes with significant risks and added costs (e.g., infection, permanent change of the body, repeated surgeries) [11], [12].

In this letter, we introduce a new interfacing method to address fitting challenges in wearable devices. Specifically, we intended this interface to be adaptive to bodies of different sizes and shapes, while being able to maintain the device-on-body structural stability required for proper functions. We achieved this through granular jamming, where the mechanical properties of an inflatable membrane filled with particles can be changed from a soft behavior to a stiff behavior by means of altering the internal air pressure. Jamming is often categorized into layer, fiber, and granular types based on the constituents; each type is suited for different applications. In particular, granular jamming structures are known to excel at conforming to objects of complex shapes [13]. Granular jamming has been popularly seen in the design of universal grippers to grasp a wider range of objects, as compared to traditional linkage-based robotic grippers [14], [15], [16]. In the wearable technology space, granular jamming has mainly been used to modulate joint stiffness and support the weight limbs [17], [18], [19]. It has also been used to design a rigid head attachment for safer image-guided surgeries [20], [21].

Leveraging its ability to switch between soft and stiff states nearly instantaneously, we propose a new application for granular jamming to design wearable attachments to allow for wider adaptability while maintaining the robot's stability during use. As illustrated in Fig. 1, a jamming layer would be integrated into

Received 26 July 2024; accepted 13 November 2024. Date of publication 4 December 2024; date of current version 9 December 2024. This article was recommended for publication by Associate Editor Seungmoon Song and Editor Yong-Lae Park upon evaluation of the reviewers' comments. This work was supported in part by the National Science Foundation (NSF) under Grant CBET 2240508 and in part by the National Institutes of Health under Grant R03HD111884. The work of Logan Lancaster was supported in part by the Research Experiences for Undergraduate program of the above funded NSF project and in part by the Undergraduate Research Opportunity Program at the University of Utah. *(Corresponding author: Haohan Zhang.)*

The authors are with the Department of Mechanical Engineering and the Robotics Center, University of Utah, Salt Lake City, UT 84112 USA (e-mail: haohan.zhang@utah.edu).

This letter has supplementary downloadable material available at https://doi.org/10.1109/LRA.2024.3511417, provided by the authors.

Digital Object Identifier 10.1109/LRA.2024.3511417

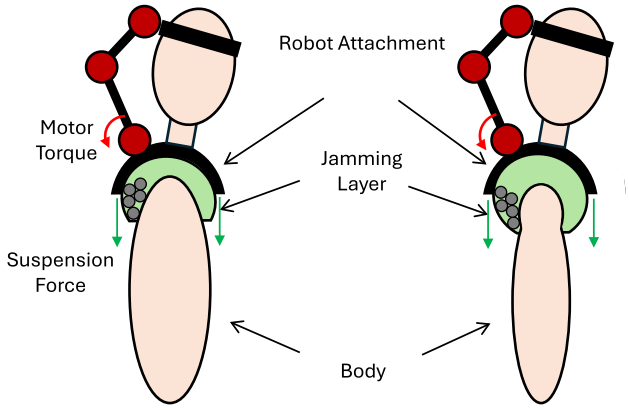

Fig. 1. Proposed shape-adaptive robot attachment using granular jamming, illustrated using the shoulder attachment of a neck exoskeleton [22] as an example. Suspension forces via elastic straps are used to secure the structure on the shoulders. During use, motors apply torques to enable head motions where forces at the interfaces will be transmitted to the shoulders.

the interfacing portion of an attachment (made of semi-rigid plastic) and could fit around the body while in its soft state. Added suspension force would strengthen the contact with the body and the jamming layer's shape adaptation. A vacuum would then be applied to change the structure to its stiff state to maintain attachment stability during use to avoid device-on-body movement, which often causes discomfort.

Our goal is to determine design parameters that maximize the ability of the system to resist external forces aimed to disrupt structural stability (e.g., torques by the actuators, forces from the environment). To this end, we designed a bench experiment that evaluated our proposed system in interactions with a group of objects of different specific shapes and sizes. A slowly increasing force was applied laterally to the jamming structure to simulate forces from the wearable device (e.g., exoskeletons) during use. We first quantified the effect of jamming (application of vacuum to jam the particles), then investigated the effects of membrane infill percentage, number of modules used in the jamming structure, and downward force exerted on the objects on the maximum force resisted by the structure. A regression model was used to explain the experimental data.

Our main contributions here are the novel design of a jamming structure for wearable interfaces that can adapt to changes and differences in human body shapes and the determination of key design parameters that will produce optimal performances. Important results from this experiment will help inform future development of jamming-based shape-adaptive attachments for wearable robots.

II. Methods

A. Overview

While several potential material choices for the granule and the membrane have been studied in the literature [23], [24], the most commonly used granules and membranes are coffee grounds and latex, respectively. In this study, we chose to keep these two materials constant while studying how other parameters contribute to resisting lateral movement. Specifically, we chose to study three variables (defined in Section II-B): amount of granule infill (*infill percentage*), area of jamming coverage as determined by the *number of modules*, and magnitude of downward suspension force (*downward force*).

We considered these parameters because they are very relevant to wearable robotics where weight, size, structural stiffness, and comfort are important [3], [25]. For example, higher granular infill and area of jamming coverage would increase the weight and size of the attachment, while higher downward suspension force and lower area of jamming coverage would increase the applied pressure on the body, thus decreasing the comfort.

We designed and built a bench model (Fig. 2) so that these parameters can be physically modified. We conducted an experiment to systematically change these parameters and use external sensors to measure the outcome variable, which is the maximum lateral disturbance force (*critical force*) for which the structure maintains its interface stability (i.e., without relative motion).

TABLE I
Independent Variables

Jammed States	Infill Percentage (i%)	Number of Modules (n_m)	Downward Force (f_d)
On	25%	1	10 N
Off	50%	2	15 N
	75%	3	20 N
	100%	4	

B. Design

This jamming structure was designed to conform around an object of varied shape and size to simulate different body sizes and contact geometries. Specifically, it was built to conform only to the lateral surface area of a cylindrical object, with the objects being longer than the jamming structure in the longitude direction. All design parameters and object configurations were physically changed for each trial (see Table I & Fig. 3).

To ensure consistency across different configurations, we chose a modular design. Each module contained one jamming membrane of a determined size and infill, as well as screw fasteners for attaching springs between the jamming structure and the inertial frame. The modules would also include tubing, attaching the membrane to a plastic hose fitting through the center of the module. By using this modular design, the flow of the granules in each module can be confined within the membrane of that module, unlike a single membrane design where an uneven distribution of granules could occur due to irreversible granule movements. This design also keeps the granules roughly in place when mounting the structure on the objects.

A vacuum pump (ZR370-02PM, Adafruit, New York, NY) and a pressure sensor (MPRLS Ported Pressure Sensor, Adafruit, New York, NY) are attached to the other end of the tubing to provide vacuum and monitor the air pressure, respectively. During each trial that jamming was applied, the pump was on constantly to ensure a consistent vacuum and avoid any unforeseen system leakages (e.g., tubing, wear and tear in balloon membranes).

1) Jammed State: This refers to the application of a vacuum. In the on or jammed state, the pump applied 100% vacuum. In the off or unjammed state, the air pressure equals the ambient air pressure.

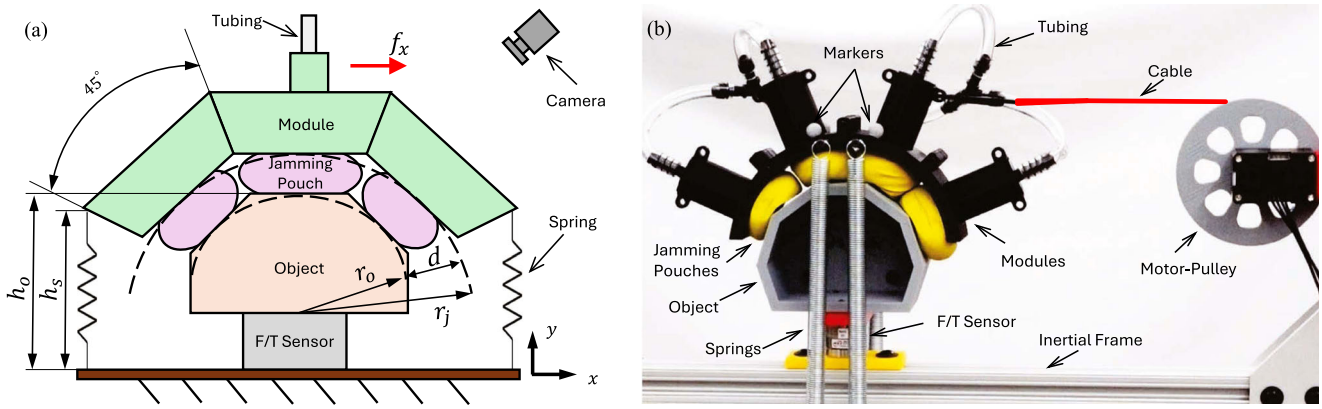

Fig. 2. Experimental setup. (a) Schematics. A lateral force f_x is applied on the module by a servomotor through a cable-pulley system. h_s shows the length of the spring, h_o represents the height of the object. r_o represents the object radius used to calculate the object size, r_j is the radius used for the jamming structure modules, and d is the distance between r_j and r_o. (b) An image showing a 4-module, 75% infill, and 15 N downward force, unjammed setup. The motor-pulley and the force/torque sensor are both fixed to an inertial frame made of 80–20 aluminum beams. Reflective markers are placed on jamming modules, objects, and the inertial frame. Four springs are attached to the jamming modules to maintain a balanced application of the downward force. The attachments of the springs on the inertial frame can be adjusted to ensure the downward force prior to data recording.

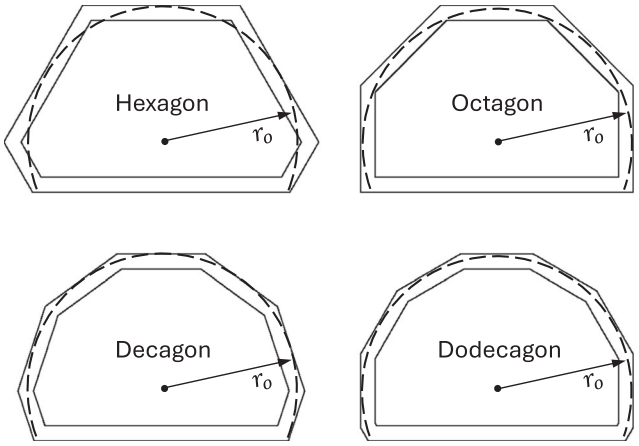

Fig. 3. Selected object shapes are shown in CAD software. Original polygons were cut to be 75 mm tall and added to the F/T sensor height (21 mm) for $h_o =$ 96 mm. Object sizes were small ($r_o = 40$ mm), medium ($r_o = 47.5$ mm), and large ($r_o = 55$ mm). The inner shape for each is a portion cutout for mounting the object to the force torque sensor.

2) Infill Percentage: The granular infill was coffee grounds (medium coarseness). Identical latex balloons (8 in. diameter at maximum rated inflation) were used for all jamming pouches. The infill percentage was calculated by subtracting the weight of the balloon from the total measured weight of the granule-filled balloon. A balloon filled to 100% of its unstretched volume weighed 16 g (measured by a scale), from which increments of 25%, 50%, and 75% were created. Each infill percentage also created a height offset between the center of the module circle with radius r_j and the center of the object circle with radius r_o (Fig. 2(a)).

3) Number of Modules: Because the membrane size was kept constant, the number of membranes was varied discretely using modules. In turn, these modules increased the contact area on the object and the total size of the device. The size of the largest object was set to have an enclosing circle of 70 mm radius, and each jamming module was designed to cover a 45° arc of the enclosing circle. We varied the number of modules from one to four in our tests, placing them as seen in Fig. 2(b). Each module was created identically except for the end pieces, which do not have the connection point for another module. The granule-filled membrane was loaded through a lofted hole in the center of a module and secured to the tubing. This design choice centers the jamming membrane under the module. All modules on each jamming structure had the same infill percentage. The weight of a single module was 30.8 g, consisting of the 3D-printed module, the tubing connector, and the nuts and bolts used to attach each module.

4) Downward Force: Wearable robotic devices are often designed to allow unrestricted movement and cannot surround the body rigidly in the target area of the device. To compensate for this, straps are often added for stability, as previously mentioned. For our device, the structure only covers a section of the lateral surface area on the object and also requires suspension force to secure the jamming structure. The suspension force was achieved through the use of extension springs attached to the middle part of the jamming structure, as seen in Fig. 2(b). This spring placement differs somewhat from straps used on a wearable device but allows consistency between the different number of modules. The rigidity of the 3D-printed parts bolted together allowed similar force distribution to other placements across all structure designs in the experiment. The combined weight of the jamming structure and the force from the springs contributed to the overall downward force measured by a force/torque (F/T) sensor (Nano 25, ATI Industrial Automation, Apex, NC). The motorized pump and tubing weight were negligible since these rested on the table on which the experiment was conducted. Because the downward force includes the jamming structure, the spring length, h_s, was adjusted to accommodate for each number of modules and each infill percentage due to weight discrepancies. The distance between the object radius, r_o, and the radius of the jamming structure, r_j, created by the membrane infill is also a contributing factor. Each structure was tested with

a downward force of 10, 15, and 20 N. The maximum downward force was chosen as 20 N by measuring the downward force of a neck exoskeleton [22] as an example of a wearable robot.

5) Object Design: Twelve 3D-printed objects of varied shapes and sizes are used to simulate different contact surfaces (Fig. 3). The sizes of the object cross-section can be related to the radius of the enclosing circle of the jamming modules (r_j) and the thickness of the jamming pouch (d),

$$r_o = r_j - d\,, \tag{1}$$

where r_o denotes the radius of the enclosing circle of the object cross-section. Note that d is dependent on the quantity of infill. In our calculation, the maximum $r_{o,\max}$ is when there is zero infill ($d = 0$), and the minimum $r_{o,\min}$ is when there is 100% infill (experimentally measured). Because we intended the jamming structure to be able to make contact on all objects when unjammed, we defined our large, medium, and small objects as when $r_o = 87\% r_{o,\max}$, $r_o = 76\% r_{o,\max}$, and $r_o = 65\% r_{o,\max}$, respectively. The depth of the cylindrical objects was designed larger than the inflatable membrane's diameter, preventing the membrane from wrapping around the object.

The object height, h_o, included the F/T sensor height and was constrained to 96 mm for all objects to reduce the variability of h_s while switching objects. This height was sufficient so that the 4-module jamming structure remained touching the object on all object sizes. The resultant object geometry is not quite a 'hexagon' or 'octagon', as a section of extra height is cut off from the bottom.

C. Experimental Procedures

As shown in Fig. 2, the six-axis F/T sensor was mounted to the inertial frame. The bias of the F/T sensor was set to 0 after an object of selected shape and size was mounted on it. Then, the modular jamming structure was placed on top of the object, unjammed (ambient pressure, soft state), and four springs were used to attach it to the inertial frame. The spring attachments were manually adjusted to ensure an even loading and a set downward force (i.e., 10, 15, or 20 N). Each membrane was checked to ensure that it would only mold to the shape of the object's lateral surface area and not around the front or back faces. In jammed trials, a vacuum was applied using the pump to jam the structure around the object. An absolute pressure of 6.5 ± 0.4 psi was verified at the beginning of each of these trials. With the pump turned on throughout the trial, the pressure was observed to maintain this value for all jammed trials.

Next, a lateral force, f_x, was applied to the object through a cable-pulley system where the force was slowly increased from 0 to 10 N, at a rate of 0.36 N/s (black dashed line in Fig. 4). The maximum lateral force of 10 N was chosen since this was the maximum value of lateral forces applied on the user's body, calculated based on the neck exoskeleton in our previous work [26]. Displacement of the jamming structure was measured by a 12-camera motion capture system (Vero, VICON, Oxford, U.K.). Reflective markers were placed on the inertial frame, the object, and the jamming structures (Fig. 2). The interface force/moment was recorded simultaneously via the six-axis F/T sensor. We first collected two blocks, one for each jammed and unjammed condition; then, we repeated an additional block on the jammed condition to have more data. Overall, a total of 1,728 trials (576 trials for each of the three blocks) were performed.

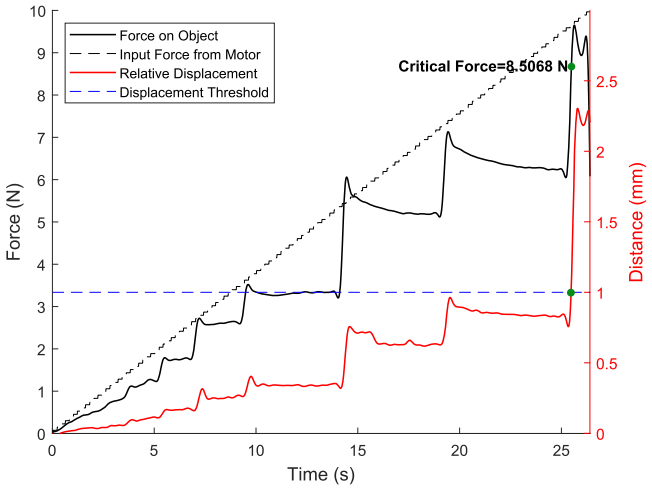

Fig. 4. Representative data of one trial. The plot shows the process of determining the critical force based on measured displacement and interface forces. The dashed black line shows the force resulting from the commanded torque to the servo motor and the pulley radius. The dashed blue horizontal line shows the 1 mm threshold, while the green dots show where on the force and displacement plots the displacement crosses the threshold. The solid black and red lines correspond to the y-axis of their same color.

D. Data Processing

The motion capture data were processed first by filling gaps using VICON Nexus (2.16.0). Then, filtering of time trajectories (force and marker) was performed in MATLAB (2023b, Mathworks, Natick, MA) using a low pass filter (passband = 1 Hz, stopband = 10 Hz). Data from the first 1.5 seconds were removed from each trial to exclude data during the cable pre-tensioning phase. The relative displacement was calculated as the change in distance between a static marker mounted to the table and a marker attached to the jamming structure.

The response variable of interest for this experiment is the critical force, defined as the amplitude of the lateral force that causes relative motion between the jamming attachment and the object. To determine this critical force value (Fig. 4), we first identify the time when a relative motion of 1.0 mm was detected. We then took the highest measured force before this time. The threshold was chosen as follows: A human operator examined video recordings of 10 randomly selected trials and determined the times at which a relative motion occurred in each trial. Then, the corresponding relative marker displacements at those times were found. The minimum displacement was 1.0 mm among the 10 trials, which was used as the threshold for all other trials.

E. Statistical Analysis

We first determined the effect of the use of jamming on the resultant critical force by running a Welch t-test, which is robust to violations of normality and homoscedasticity [27],

TABLE II
FINAL REGRESSION MODEL*

Variable**	Estimate	95% CI	p value
β_0 - (Intercept)	**1.821**	**[1.246 2.396]**	**7.40e-10**
β_1 - $i\%$	**-0.023**	**[-0.028 -0.018]**	**< 2e-16**
β_2 - $n_m = 2$	**1.814**	**[1.001 2.628]**	**1.33e-5**
β_3 - $n_m = 3$	**2.687**	**[1.873 3.501]**	**1.37e-10**
β_4 - $n_m = 4$	**1.885**	**[1.071 2.699]**	**6.059e-6**
β_5 - f_d	**0.220**	**[0.189 0.252]**	**< 2e-16**
β_6 - i%:$n_m = 2$	-0.004	[-0.010 0.003]	0.282
β_7 - i%:$n_m = 3$	**0.018**	**[0.011 0.024]**	**1.620e-7**
β_8 - i%:$n_m = 4$	**0.013**	**[0.0065 0.0197]**	**1.00e-4**
β_9 - $n_m = 2$:f_d	**0.065**	**[0.020 0.111]**	**0.005**
β_{10} - $n_m = 3$:f_d	1.32e-4	[-0.045 0.045]	0.995
β_{11} - $n_m = 4$:f_d	0.013	[-0.032 0.059]	0.560

* Significant coefficients are in bold.
** $i\%$ = infill percentage, n_m = number of modules, f_d = downward force

TABLE III
SUCCESSFUL GRIPS IN THE CASE STUDY*

Infill Percentage	Downward Force (N)	Number of Modules 1	2	3	4
25%	10	0	7	11	5
25%	15	0	12	12	10
25%	20	7	12	12	12
50%	10	0	2	2	8
50%	15	0	12	10	12
50%	20	3	12	11	12
75%	10	0	2	11	6
75%	15	0	7	12	12
75%	20	1	12	12	12
100%	10	0	0	8	3
100%	15	0	3	12	7
100%	20	0	11	12	12

* Darker shades highlight more successful grips.

[28], comparing the critical forces in the first two blocks. The statistical significance level was set to be $\alpha = 0.05$.

Then, we used a linear regression model to evaluate the effect of three additional design parameters (infill percentage, number of modules, and downward force) on the critical force under the jammed condition. Infill percentage and downward force were modeled as continuous independent variables, while the number of modules n_m was modeled as a categorical variable, with $n_m = 1$ as the reference level. As described in Section II-B, we sampled at four levels for the infill percentage (25%, 50%, 75%, and 100%) and the number of modules (one to four modules placed as shown in Fig. 2), and at three levels for the downward force (10, 15 and 20 N). Each jamming structure, identified by a unique combination of the parameters mentioned above, was tested on twelve different objects with two repetitions, with a total of 1,152 trials. We started by considering the full model with up to three-way interactions and used backward elimination to narrow down to a parsimonious model [29] based on significance.

III. RESULTS

Critical force values of jammed trials were significantly different from unjammed trials ($p < 0.001$) with an effect size of 1.94 N ([1.73 2.17] 95% confidence interval). The unjammed trials had an average critical force value of 4.09 N, while the jammed trials had an average critical force value of 6.04 N.

Table II shows the final parsimonious model that was produced as an output of the backward elimination model selection after we found that the three-way interactions between all factors and the two-way interaction between infill percentage and downward force were not significant. The top half of Fig. 5 shows box plots for the main effects of factors (infill percentage, number of modules, and downward force) on the dependent variable critical force (as a reminder, this data was obtained in the jammed state). Significant main effects were found for all three factors. The number of modules had the largest effect on the critical force, with three modules showing the largest increase of 2.687 N on the critical force when compared to the reference level (one module). The downward force and infill had smaller but still significant effects on the critical force, with higher downward forces increasing the critical force (0.22 N increase on the critical force per 1 N increase on the downward force) and higher infill percentages decreasing the critical force (-0.023 N per infill percent).

Additionally, some of the module configurations had small but significant interaction effects with infill percentages and downward forces. The lower half of Fig. 5 shows interaction plots, with a focus on the interaction between number of modules and infill percent that is particularly noticeable for a 50% infill (the critical force decreases for 3 modules, which otherwise causes it to increase at different infill levels). This interaction was further investigated with a posthoc test comparing means from changes in the number of modules at the four fixed levels of infill, with Tukey-adjusted p-values as provided by the `emmeans` package in R. All pairwise comparisons yielded $p <= 0.0001$, except for the following: $n_m = 2$ vs $n_m = 3$ for 50% infill (p = 0.0272), $n_m = 3$ vs $n_m = 4$ for 75% infill (p = 0.0007), and $n_m = 2$ vs $n_m = 4$ for 100% infill (p = 0.0954), which was the only paired comparison to not be significant at the 5% significance level.

Lastly, to demonstrate and compare the ability of each jamming design to adapt to different objects, we created the following case scenario: assuming a set critical force at 6 N, which was the average value of the jammed trials, we counted the number of objects that each design can maintain the set force, as summarized in Table III. The maximum number of objects is 12 due to the number of sizes and shapes of the objects. Using this table, one can identify parameter combinations for designs that are more likely to be successful in adapting to a wider range of objects with a target structural stability. For example, a design with 2 modules, 25% infill, and a downward force of 15 N was able to resist the set critical force for all 12 tested objects. Similarly, a design with 3 modules, 100% infill, and a downward force of 20 N achieved the same. With this set critical force, the table also shows that 1-module designs are most likely to fail, only with moderate success when the infill percentage is low (25%) and the downward force is high (20 N).

IV. DISCUSSION

Our experiment shows that jamming (vacuum) is necessary to provide a higher ability of the structure to resist lateral

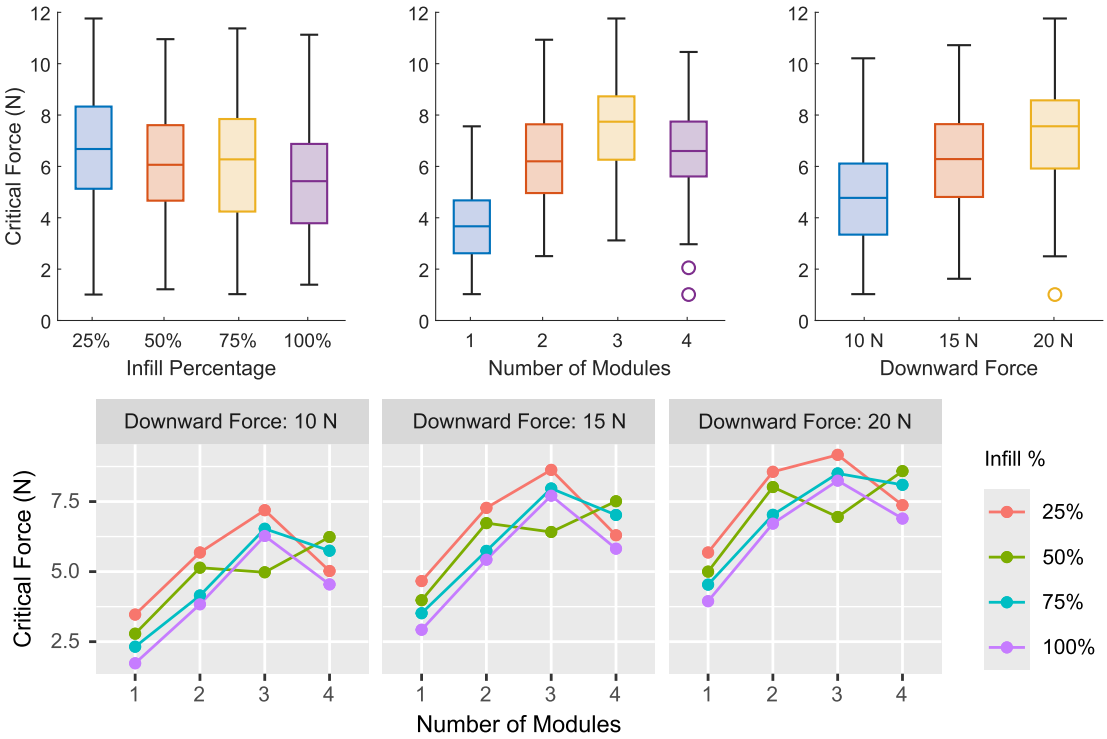

Fig. 5. Top: box plots of *percentage infill*, *number of modules*, and *downward force* vs. *critical force* for jammed trials. Bottom: interaction plots for the number of modules and percentage infill.

disturbance. Although unjammed structures are not commonly used, they are somewhat similar to using padding materials (e.g., foam) that have low, constant stiffness. When unjammed, the membrane(s) of the structure displayed a slipping or rolling motion upon displacement. This behavior is expected due to the lower stiffness and pliable composition of granule-filled membranes. The structure still conforms to shape, especially if there is a downward suspension force keeping it on the target object. By contrast, jammed structures appeared to be rigidly attached to the objects until a breaking point where the structure was displaced. If the jamming structure was displaced yet remained on the object, the shape of the jamming pouches would remain intact and the device could not remold to the object in its displaced position, unlike the unjammed cases.

Within this experiment, there were cases observed where an unjammed structure outperforms a jammed structure in terms of higher critical force. For example, an unjammed 3-module structure has, on average, a higher critical force than that of a jammed 1-module structure. This behavior is likely caused by the difference in underlying mechanics. In the 1-module case, the structure does not have a large enough contact area to reach the edges of each object's lateral surface area. Without edges to grip onto, the only force keeping the jamming structure on the object is the friction between the object and membrane, which is mostly determined by the amount of downward force (given fixed material properties). In contrast, a 3-module unjammed structure would have a higher contact area that can grip on the sides of the object, which creates an additional normal force to the side to resist the lateral pull. As a result, even when the 3-module structure was unjammed, it still generated higher resistance.

The difference in mechanics for structures with different numbers of modules also explains the largest effect of the number of modules on the critical force in our model. Interestingly, a higher number of modules does not always mean higher critical force, as we show that the 3-module designs generally yielded higher critical force than the 4-module structures, with the only exception for this being observed for the 50% infill because of the significant interaction effect between infill percentage and number of modules. A likely explanation is that a 4-module design did not always create equal contact with the objects among all jamming pouches, causing the contact force to distribute unevenly. This was more profound in small and large object cases. The pouches barely made contact with the small objects in all directions, and the large objects left limited space for the jamming pouches to conform to the surfaces. By contrast, the 3-module designs seem to have the best performance for all objects tested.

We also observed that a higher downward force increases the critical force. This influence of the downward force on the critical force was nearly linear. This is not surprising, as a higher downward force produces a higher friction force, which is one of the main forces to resist lateral disturbance, as mentioned above. One additional note to the downward force is that it is the sum of the weight of the attachments plus the added suspension force from the springs. In our experiment, we carefully adjusted springs for each trial so that the total downward force equaled the target set force. Our result does not differentiate the effects of these two downward forces.

We expected that there is an optimal amount of granule infill to produce the highest critical force, given that when the infill is zero or 100%, the jamming structure is nearly rigid and thus not adaptive to shapes. However, we observed that a lower amount of granule infill always improves the critical force, although the influence of this variable is the lowest among the three variables studied. This result also means that there is possibly an optimal infill percentage between zero and 25%, although we cannot verify this with our current data. Nonetheless, less granule infill could be beneficial for attachment design as it makes the device lighter.

Small but significant interaction effects were found between the number of modules and infill percentage and between the number of modules and the downward force. In particular, interactions between three modules and infill percentage and between four modules and infill percentage were large enough to essentially counteract the negative main effect from the infill percentage. From the physical model design standpoint, this could be partially caused by the (unintended) contact between adjacent jamming pouches in configurations with multiple modules that have higher infill percentages (Fig. 2(b)).

While the linear regression model helps predict the critical force given a set of design parameters, we also created an example scenario to identify designs that can adapt to the most objects of various shapes and sizes for a target critical force. We showed that there are often multiple plausible design choices. A designer may further select an optimal design given other factors that are pertinent to their applications. For example, one may choose a 2-module design over a 3-module one due to the reduced size and weight of the structure; or choose a 15 N downward force rather than 20 N downward force due to less pressure applied on the wearer.

We acknowledge that the metric of critical force may differ from representations of performance indicators used in the related literature [13], [14], [18], [21]. While the force-displacement relationship of each structure was important, quantifying the performance of each jamming structure by one force value would allow for comparison across the 576 jamming structures used in this design-motivated experiment.

We used a thresholding method to determine the time when a relative motion (slippage) happens between the jamming modules and the object. The choice of threshold would affect the calculation of the critical force. In our study, we elected to rely on the detection of a human. The rationale for this is that although micro-displacements (relative motion less than detected by a human) could occur, they may not be critical to the target application of wearable attachment design, where larger relative motions are more likely to affect comfort and device function. During our pilot experimental phase, we also evaluated alternative thresholding methods, such as relying on the maximum displacement of stationary markers on the inertial frame, which would reflect the measurement noise of the motion capture. However, this method was too conservative, where video footage showed visible movement of the jamming structure after the time detected by this thresholding method.

For the proposed application, a limitation of this study is that only 3D-printed standard objects were used. Using the assumption that most areas of the body where wearable robotics would be attached could be modeled as elliptical or cylindrical [30], these objects were varied in size and roundness for representing parts of the body this type of jamming structure could be applied. Although the size and shape of the objects were varied, they are all rigid, which are less accurate representations of parts of the body that have layers of fat and muscles. For bony areas of the body, such as shoulders, pelvis, forehead, and shins, the current results may be most translatable. Another limitation was that the applied force perturbation was only in one direction and was nearly quasi-static. Hence, three-dimensional force-moment and dynamic effects that could occur in an actual human-robot interaction were not studied. Future implementations of the results of this letter to design wearable attachments will be carried out and tested on human users in more realistic use scenarios, which would provide further evidence of the extent to which the proposed jamming-based attachment would address the fitting challenge in wearable devices. Beyond the proposed application, our methodology and results could provide insights for other jamming applications, such as the evaluation of granular jamming grippers to resist lateral force perturbations from the environment.

In future applications, the system design needs to be airtight to prevent leakages. This will be important for the jamming structure to maintain a vacuum so that the constant vacuum through a pump is unnecessary. The vacuum pump creates noise while powered on that may be disturbing for the user. By sealing the air vacuum in the device, the pump could be powered off once the membranes are jammed. Avoiding using the pump more than necessary reduces the power required for the vacuum pump. Additionally, work on modular designs could be explored to better adapt to specific applications on the body or outside of wearable robotics. Modular designs also provide flexibility for sizing the jamming structure for intended applications. With these modifications, extra tubing may be needed, and the air seals on each membrane would need to be carefully designed and fabricated.

V. Conclusion

This letter presented results from the first experiment, designed to measure the effects of parameters of a granular jamming structure to adapt to the sizes and shapes of different objects while providing lateral stability. This experiment aimed to simulate the attachment of wearable devices using this novel approach to interface with the human body with complex shapes and different sizes. Future work will involve the implementation of this bench model into a physical design for wearable devices (e.g., the Utah Neck Exoskeleton [26]) and evaluate the design with human participants to demonstrate the effectiveness of such a wearable interface to adapt to complex body shapes.

References

[1] F. Porciuncula et al., "Wearable movement sensors for rehabilitation: A focused review of technological and clinical advances," *PM&R*, vol. 10, pp. S220–S232, Sep. 2018. [Online]. Available: https://www.sciencedirect.com/science/article/pii/S1934148218303630

[2] D. Pinto-Fernandez et al., "Performance evaluation of lower limb exoskeletons: A systematic review," *IEEE Trans. Neural Syst. Rehabil. Eng.*, vol. 28, no. 7, pp. 1573–1583, Jul. 2020. [Online]. Available: https://ieeexplore.ieee.org/abstract/document/9103122

[3] M. Zhu et al., "Soft wearable robotics and haptics: Technologies, trends, and emerging applications," *Proc. IEEE*, vol. 110, no. 2, pp. 246–272, Feb. 2022. [Online]. Available: https://ieeexplore.ieee.org/abstract/document/9686045

[4] J. Tamez-Duque, R. Cobian-Ugalde, A. Kilicarslan, A. Venkatakrishnan, R. Soto, and J. L. Contreras-Vidal, "Real-time strap pressure sensor system for powered exoskeletons," *Sensors*, vol. 15, no. 2, pp. 4550–4563, Feb. 2015. [Online]. Available: https://www.mdpi.com/1424-8220/15/2/4550

[5] A. Schiele and F. C. T. van der Helm, "Kinematic design to improve ergonomics in human machine interaction," *IEEE Trans. Neural Syst. Rehabil. Eng.*, vol. 14, no. 4, pp. 456–469, Dec. 2006. [Online]. Available: https://ieeexplore.ieee.org/document/4032758

[6] V. Dhokia, J. Bilzon, E. Seminati, D. C. Talamas, M. Young, and W. Mitchell, "The design and manufacture of a prototype personalized liner for lower limb amputees," *Procedia CIRP*, vol. 60, pp. 476–481, Jan. 2017. [Online]. Available: https://www.sciencedirect.com/science/article/pii/S2212827117302846

[7] M. A. de Souza, C. Schmitz, M. M. Pinhel, J. A. Palma Setti, and P. Nohama, "Proposal of custom made wrist orthoses based on 3D modelling and 3D printing," in *Proc. 39th Annu. Int. Conf. IEEE Eng. Med. Biol. Soc.*, 2017, pp. 3789–3792. [Online]. Available: https://ieeexplore.ieee.org/abstract/document/8037682

[8] J. M. Munoz-Guijosa, R. Zapata Martínez, A. Martínez Cendrero, and A. Díaz Lantada, "Rapid prototyping of personalized articular orthoses by lamination of composite fibers upon 3D-Printed molds," *Materials*, vol. 13, no. 4, Jan. 2020, Art. no. 939. [Online]. Available: https://www.mdpi.com/1996-1944/13/4/939

[9] W. Flanagan et al., "Prosthetic limb attachment via electromagnetic attraction through a closed skin envelope," *IEEE Trans. Biomed. Eng.*, vol. 71, no. 5, pp. 1552–1564, May 2024.

[10] R. P. Brånemark, K. Hagberg, K. Kulbacka-Ortiz, Ö. Berlin, and B. Rydevik, "Osseointegrated percutaneous prosthetic system for the treatment of patients with transfemoral amputation: A prospective five-year follow-up of patient-reported outcomes and complications," *JAAOS- J. Amer. Acad. Orthopaedic Surgeons*, vol. 27, no. 16, pp. e743–e751, 2019.

[11] J. Tillander, K. Hagberg, L. Hagberg, and R. Brånemark, "Osseointegrated titanium implants for limb prostheses attachments: Infectious complications," *Clin. Orthopaedics Related Res.*, vol. 468, no. 10, pp. 2781–2788, 2010.

[12] G. Tsikandylakis, Ö. Berlin, and R. Brånemark, "Implant survival, adverse events, and bone remodeling of osseointegrated percutaneous implants for transhumeral amputees," *Clin. Orthopaedics Related Res.*, vol. 472, pp. 2947–2956, 2014.

[13] B. Aktaş, Y. S. Narang, N. Vasios, K. Bertoldi, and R. D. Howe, "A modeling framework for jamming structures," *Adv. Funct. Mater.*, vol. 31, no. 16, 2021, Art. no. 2007554. [Online]. Available: https://onlinelibrary.wiley.com/doi/abs/10.1002/adfm.202007554

[14] E. Brown et al., "Universal robotic gripper based on the jamming of granular material," *Proc. Nat. Acad. Sci.*, vol. 107, no. 44, pp. 18809–18814, Nov. 2010. [Online]. Available: https://www.pnas.org/doi/abs/10.1073/pnas.1003250107

[15] Y. Wei et al., "A novel, variable stiffness robotic gripper based on integrated soft actuating and particle jamming," *Soft Robot.*, vol. 3, no. 3, pp. 134–143, Sep. 2016. [Online]. Available: https://www.liebertpub.com/doi/full/10.1089/soro.2016.0027

[16] T. Joseph, S. Baldwin, L. Guan, J. Brett, and D. Howard, "The jamming donut: A free-space gripper based on granular jamming," in *Proc. IEEE Int. Conf. Soft Robot.*, 2023, pp. 1–6. [Online]. Available: https://ieeexplore.ieee.org/document/10121993

[17] S. Hauser, M. Robertson, A. Ijspeert, and J. Paik, "JammJoint: A variable stiffness device based on granular jamming for wearable joint support," *IEEE Robot. Automat. Lett.*, vol. 2, no. 2, pp. 849–855, Apr. 2017. [Online]. Available: https://ieeexplore.ieee.org/document/7823007

[18] T. Liu, H. Xia, D.-Y. Lee, A. Firouzeh, Y.-L. Park, and K.-J. Cho, "A positive pressure jamming based variable stiffness structure and its application on wearable robots," *IEEE Robot. Automat. Lett.*, vol. 6, no. 4, pp. 8078–8085, Oct. 2021. [Online]. Available: https://ieeexplore.ieee.org/abstract/document/9484778

[19] S. Zuo, H. Li, Z. Hua, J. Liu, and B. Chen, "A novel jamming structure with interlocking mechanism towards applications in wearable robots," *IEEE Robot. Automat. Lett.*, vol. 7, no. 3, pp. 6305–6312, Jul. 2022. [Online]. Available: https://ieeexplore.ieee.org/abstract/document/9754274

[20] P. S. Wellborn, N. P. Dillon, P. T. Russell, and R. J. Webster, "Coffee: The key to safer image-guided surgery–a granular jamming cap for non-invasive, rigid fixation of fiducial markers to the patient," *Int. J. Comput. Assist. Radiol. Surg.*, vol. 12, no. 6, pp. 1069–1077, Jun. 2017. [Online]. Available: https://www.ncbi.nlm.nih.gov/pmc/articles/PMC6252059/

[21] R. Wirz, R. A. Lathrop, I. S. Godage, J. Burgner-Kahrs, P. T. R. Iii, and R. J. W. Iii, "Can coffee improve image guidance?" in *Proc. Med. Imag., Image-Guided Procedures, Robotic Interv., Model.*, 2015, pp. 257–268. [Online]. Available: https://www.spiedigitallibrary.org/conference-proceedings-of-spie/9415/941513/Can-coffee-improve-image-guidance/10.1117/12.2082965.full

[22] H. Zhang and S. K. Agrawal, "An active neck brace controlled by a joystick to assist head motion," *IEEE Robot. Automat. Lett.*, vol. 3, no. 1, pp. 37–43, Jan. 2018.

[23] S. G. Fitzgerald, G. W. Delaney, and D. Howard, "A review of jamming actuation in soft robotics," *Actuators*, vol. 9, no. 4, Dec. 2020, Art. no. 104. [Online]. Available: https://www.mdpi.com/2076-0825/9/4/104

[24] A. Jiang et al., "Robotic granular jamming: Does the membrane matter?" *Soft Robot.*, vol. 1, no. 3, pp. 192–201, Sep. 2014. [Online]. Available: https://www.liebertpub.com/doi/10.1089/soro.2014.0002

[25] F. Yakub, A. Z. Md Khudzari, and Y. Mori, "Recent trends for practical rehabilitation robotics, current challenges and the future," *Int. J. Rehabil. Res.*, vol. 37, no. 1, pp. 9–21, Mar. 2014.

[26] D. Demaree and H. Zhang, "A structurally enhanced neck exoskeleton to assist with head-neck motion," in *Proc. Int. Symp. Med. Robot.*, Apr. 2023, pp. 1–7. [Online]. Available: https://ieeexplore.ieee.org/abstract/document/10130255

[27] J. M. Stonehouse and G. J. Forrester, "Robustness of the t and U tests under combined assumption violations," *J. Appl. Statist.*, vol. 25, no. 1, pp. 63–74, 1998.

[28] M. Delacre, D. Lakens, and C. Leys, "Why psychologists should by default use Welch's t-test instead of student's t-test," *Int. Rev. Social Psychol.*, vol. 30, no. 1, pp. 92–101, 2017.

[29] C. Lindsey and S. Sheather, "Variable selection in linear regression," *Stata J.*, vol. 10, no. 4, pp. 650–669, 2010.

[30] R. H. Crompton, Y. Li, R. M. Alexander, W. Wang, and M. M. Gunther, "Segment inertial properties of primates: New techniques for laboratory and field studies of locomotion," *Amer. J. Phys. Anthropol.*, vol. 99, no. 4, pp. 547–570, 1996.